Aircraft Charging and its Influence on Triggered Lightning

JGR Atmospheres

RESEARCH ARTICLE
10.1029/2019JD031245

Aircraft Charging and its Influence on Triggered Lightning

C. Pavan[1], P. Fontanes[2], M. Urbani[2], N. C. Nguyen[1], M. Martinez-Sanchez[1], J. Peraire[1], J. Montanya[2], and C. Guerra-Garcia[1]

[1]Department of Aeronautics and Astronautics, Massachusetts Institute of Technology, Cambridge, MA, USA, [2]Department of Electrical Engineering, Universitat Politècnica de Catalunya, Terrassa (Barcelona), Spain

Key Points:
- Aircraft-triggered lightning is influenced by the net charge of the floating body
- Positive leader inception from an aircraft requires higher amplitude external fields when negatively biasing the vehicle
- Experimental results validate a proposed method of aircraft-triggered lightning strike risk reduction

Correspondence to:
C. Guerra-Garcia,
guerrac@mit.edu

Citation:
Pavan, C., Fontanes, P., Urbani, M., Nguyen, N. C., Martinez-Sanchez, M., Peraire, J., et al. (2020). Aircraft charging and its influence on triggered lightning. *Journal of Geophysical Research: Atmospheres*, *125*, e2019JD031245. https://doi.org/10.1029/2019JD031245

Received 1 JUL 2019
Accepted 17 DEC 2019
Accepted article online 20 DEC 2019

Abstract This paper reports on a laboratory experiment to study the effect of vehicle net charge on the inception of a positive leader from an aircraft exposed to high atmospheric electric fields. The experiment models the first stage of aircraft-triggered lightning in which a positive leader typically develops from the vehicle and is shortly afterwards followed by a negative leader. This mechanism of lightning initiation amounts to around 90% of strikes to aircraft. Aircraft can acquire net charge levels of the order of a millicoulomb from a number of sources including corona emission, charged particles in the engine exhaust, and charge transfer by collisions with particles in the atmosphere. In addition, aircraft could potentially be artificially charged through controlled charge emission from the surface. Experiments were performed on a model aircraft with a 1m wingspan, which was suspended between two parallel electrodes in a 1.45m gap with voltage difference of a few hundred kilovolts applied across it. In this configuration, it is found that the breakdown field can vary by as much as 30% for the range of charging levels tested. The experimental results show agreement with an electrostatic model of leader initiation from aircraft, and the model indicates that the effect can be substantially stronger if additional negative charge is added to the aircraft. The results from this work suggest that flying uncharged is not optimal in terms of lightning avoidance and open up the possibility of developing risk-reduction strategies based on net charge control.

Plain Language Summary Commercial aircraft are typically struck by lightning around once per year, and the vast majority of these events are triggered by the aircraft itself. The lightning discharge originates on the surface of the aircraft in areas with sharp edges. Whether a discharge develops is in part due to the net electric charge of the aircraft, which can be acquired both naturally or artificially. Previous work has shown that it is theoretically possible to reduce the likelihood of a lightning strike occurring by manipulating the net charge of the aircraft. In this paper, the authors perform laboratory experiments to validate this hypothesis. These experiments demonstrate that the threshold for lightning could be increased by 30% by charging the aircraft negatively, which means that an aircraft could fly safely through ambient electric fields that are around 30% higher than those of an uncharged baseline. Theoretical estimates suggest that further improvement may be possible if the aircraft were charged to a more negative state than those tested. This work gives laboratory scale experimental evidence that it is possible to reduce the frequency of lightning strikes on aircraft by manipulating their charge and encourages further investigation of the proposed lightning strike risk reduction strategy.

1. Introduction

Formal studies into lightning effects and aircraft survivability began in the 1940s after the catastrophic accident of a Pennsylvania-Central Airlines DC-3A aircraft (Plumer, 2017). Nowadays, strict *protection and mitigation* measures are embedded in aircraft: the use of expanded metal foil or wire mesh to ensure a fully conductive path and electromagnetic shielding in composite structures, incorporation of lightning diverter strips in the radome, securing of fasteners and joints to avoid arcing and sparking in the fuel tanks, wire bundle shielding, proper grounding, and the use of surge protectors (Sweers et al., 2012). These measures ensure the safety of flight in the event of a strike and must comply with regulations of the civil certification authorities (the Federal Aviation Administration, FAA, and the European Aviation Safety Agency, EASA). Standard committees (the Society of Automotive Engineers, SAE, and the European Organization for Civil Aviation Equipment, EUROCAE) provide detailed guidelines on testing standards to demonstrate compli-

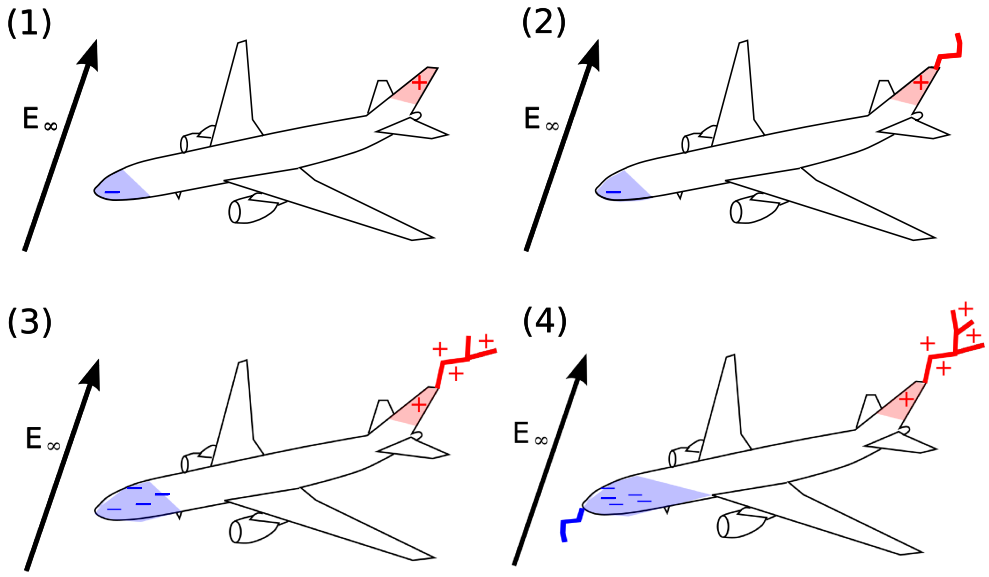

Figure 1. Bidirectional uncharged leader formation from an aircraft exposed to atmospheric electric fields. See the fourth paragraph of section 1 for detailed discussion.

ance (section 2.1). Although lightning strikes pose no critical safety concerns, they are responsible for costly delays, service interruptions, and repairs.

It is generally quoted that, on average, commercial aircraft are struck by lightning about once per year, a figure that is supported by both instrumented flight campaigns and commercial operations (Fisher & Plumer, 1977). The frequency of lightning strikes that a particular aircraft experiences will of course depend on factors such as its flight envelope (geographic area of operation, cruise altitude, duration of climb, and descent) and size.

From an *operational perspective*, the highest probabilities for lightning strikes have been observed during climb and descent at an altitude of 5,000–15,000 ft. Most lightning strikes to airplanes occur close to freezing temperatures and during precipitation but not necessarily in the presence of an active thunderstorm (Rakov & Uman, 2003).

From an *electrostatic perspective*, lightning initiation from aircraft, or *aircraft-triggered lightning* (Moreau et al., 1992), can be explained using the bidirectional uncharged leader concept (Kasemir, 1950; Mazur, 1988; 1989). This mechanism, responsible for about 90% of strikes, was verified using airborne data from the NASA F-106B (Fisher & Plumer, 1984) and FAA CV-580 (Reazer et al., 1987) campaigns. The sequence of events that precede a lightning strike is shown schematically in Figure 1: (1) the aircraft is polarized when exposed to atmospheric electric fields, resulting in the amplification of the local electric fields at its extremities; (2) a positive leader is triggered due to the lower inception and propagation thresholds for the positive polarity; (3) charge conservation forces the aircraft to more negative charge levels, further enhancing the local electric fields at the negatively charged extremities; (4) finally, the threshold for negative leader inception and propagation is reached, and a negative leader follows. If the leaders connect with others originating from clouds or the ground, a damaging high current arc forms. Viewed from this electrostatic perspective (Lalande et al., 1999a), to first order, the probability of aircraft-triggered lightning will only depend on the geometry of the vehicle, the external fields, the atmospheric conditions (which will modify the inception thresholds), and the net vehicle charge.

In this work the influence of the vehicle's net charge on leader inception is experimentally demonstrated, confirming recent theoretical estimates by (Guerra-Garcia et al., 2017, 2018). These results are relevant since aircraft can acquire net charge from a number of sources including friction with the runway during takeoff, corona discharges from static dischargers or other electrically stressed regions, charged species in the engine exhaust, and charge transfer by collision with particles in the atmosphere (Vonnegut & Little, 1965). In addition, the results from this work may open up a pathway towards an active means of reducing the risk of aircraft-triggered lightning through charge control (Martinez-Sanchez et al., 2019).

The paper is organized as follows. It begins with an overview of aircraft lightning leader attachment testing standards, followed by a description of the modifications incorporated to allow for the exploration of the effect of the vehicle's net charge. Next, experimental results of the dependence of lightning inception on aircraft charge are presented and compared to a theoretical model. The paper closes with a discussion on how the *electrostatic perspective* of aircraft-triggered lightning can assist the development of lightning *detection and prediction*, and ultimately, *risk reduction* technologies.

2. Testing Procedures

2.1. Overview of Lightning Leader Attachment Testing

Aircraft components must undergo a variety of tests for susceptibility to environmental damage. In particular, testing standards representative of flight conditions leading up to and during a strike are described in the SAE standard ARP5416 (SAE Aerospace, 2005) and the equivalent European standard EUROCAE ED-105 (EUROCAE, 2005). The impact of strikes to aircraft are typically classified as either direct effects, encompassing any risks associated with the lightning discharge itself, or indirect effects, which arise from interactions between the electromagnetic fields generated by the discharge and components of the aircraft. Direct effects mostly correspond to physical damage to the external surfaces of the aircraft, while indirect effects include damage to sensors and electronics (Plumer, 2012; Uman, 2008).

The risks associated with lightning strikes can also be broken up chronologically since, in most cases, the lightning channel attachment location will be swept along the aircraft as a result of its motion. This can result in lightning damage occurring on locations of the aircraft that are not leader trigger points themselves (Lalande & Delannoy, 2012). In general, aircraft are divided into zones based on how they typically experience lightning strikes. The locations corresponding to initial leader connection and first return stroke are referred to as zone 1 per guidelines given in SAE standard ARP5414 (SAE Aerospace, 2012). While determination of the extent of this zone requires in-depth analysis and testing, it generally encompasses most of the aircraft extremities, which will enhance the local electric field and favor leader initiation. Examples include the aircraft nose, wingtips, nacelles, and empennage. Zone 2 corresponds to regions susceptible to subsequent return strokes as the lightning channel is swept along the aircraft and zone 3 to regions experiencing current flow without arc attachment (SAE Aerospace, 2012).

Lightning leader and swept channel attachment tests are conducted by applying different high voltage waveforms across a gap containing the components to be tested. The voltage required depends on the size of the gap but will be on the order of hundreds of kilovolts to a few megavolts. The currents produced in these tests are relatively low (for the experiments reported, the generator provides about 800A); hence, these tests are used to determine leader attachment locations only and not for determining potential damage (SAE Aerospace, 2005). Damage assessment is performed by applying a sequence of high-current waveforms directly to the component. These current waveforms replicate the many individual current pulses resulting from first return stroke, continuing current and subsequent return strokes following the initial leader connection (SAE Aerospace, 2005).

In this work, the primary concern is lightning initiation; the relevant testing standards to determine the initial attachment of a lightning leader are described in section 5.1.1 of ARP5416(SAE Aerospace, 2005). The background electric field amplitude dependence with time, recommended for this test, is a D-type waveform as specified by SAE standard ARP5412 (SAE Aerospace, 2013). This waveform has a rise time of 50–250μs and a decay to half-maximum time on the order of 2ms. It is designed to increase at a slow enough rate so as to allow streamer coronae to develop and propagate from the aircraft, which results in a greater variation of lightning attachment points to the model (Plumer, 2012; SAE Aerospace, 2013). The experimental setup to demonstrate the influence of net charge on aircraft-triggered lightning is based on this standard and is described in section 2.2.

2.2. Experimental Setup

Lightning leader attachment tests make use of a conductive model aircraft suspended between two electrode plates, one grounded, one at high voltage, to simulate the effect of a strong ambient field on a vehicle in flight.

A diagram of the experimental setup is shown in Figure 2, and a plan view showing the approximate locations of the sensors is shown in Figure 3. A high-voltage plate 2m in diameter was suspended 145cm above a

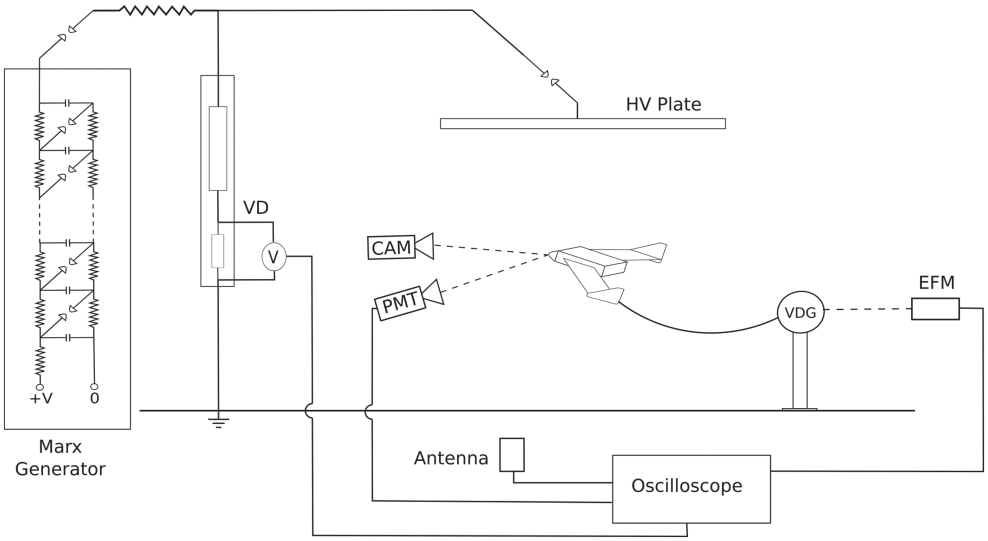

Figure 2. Diagram of experimental setup to demonstrate effect of model net charge on first leader inception. Dashed lines are noncontact line-of-sight measurements. PMT = photomultiplier tube, EFM = electric field mill, VD = voltage divider, VDG = Van de Graaff generator, CAM = camera.

grounded base. The high-voltage electrode was connected to a 1MV Marx generator through a resistor with a spark gap on either side. Between the resistor and the spark gap to the electrode, a damped capacitive voltage divider was connected to measure the applied voltage. Two lengths of kevlar rope were strung through the gap between the high-voltage electrode and ground plate, and the test model was rested on them. The rope was secured at either end to PTFE (polytetraflouroethylene) blocks, which were anchored to ground. The test model was pitched up with an angle between the nose and the ground of approximately 50degrees. The shortest distance between the model aircraft and the high-voltage plate was 26cm measured at the aircraft nose, and the shortest distance between the model and the ground was 78cm measured at the winglets. This orientation was chosen to favor positive leader formation from the nose of the model (rather than, for example, the wing tips) so that there would be a repeatable location on which to focus optical sensors. The model itself was electrically connected via conducting wire to a Van de Graaff generator, which provided a means of charging the floating body to tens of kilovolts (negative) relative to ground. The Van de Graaff generator was operated using batteries to keep it separated from the building electrical system and in this setup could sustain a model potential of up to –40kV. The Van de Graaff generator remained on for the duration of the test. The smooth spherical geometry of the Van de Graaff top electrode provided a good reference surface on which to focus an electric field mill to get a noncontact measurement of this potential. This sphere was mounted on top of an insulating post designed to allow voltages of up to –400kV relative to the grounded base without electric breakdown or significant current conduction.

The model aircraft used for this experiment was the frame of a hobby aircraft constructed to dimensions given by Bixler and Sponholz (2016). The model was a blended-wing-body design approximately 52cm in length with a wingspan of 104cm and a radius of curvature of 2.5cm at the nose. The entire model was wrapped in aluminum foil to ensure conductivity.

In this work, three different high-voltage waveforms (applied to the upper plate) were tested including a D-type waveform (with rise time 90μs, waveform 1) and two waveforms with longer rise times (waveforms 2 and 3 with rise times of 330μs and 800μ s, respectively). The rise time is here defined as the time to peak. Negative amplitude waveforms were applied in this experiment so that the aircraft model would be positively charged relative to the high-voltage plate, and thus, the positive leader would originate from the model aircraft. The waveforms are shown if Figure 4 with a normalized peak amplitude in order to compare rise and decay times; in the experiments, the peak amplitude was varied as part of the up and down method described in section 2.4. Figure 4 shows both the idealized waveforms and actual measured signals. Note that the measured signals show spikes during the initial rise and during the decay. These spikes are the result of the spark gap to the HV plate turning on and off. The voltage measured through the voltage divider is equal to the voltage on the plate while this spark gap is closed; for example, in waveform 3, between approximately

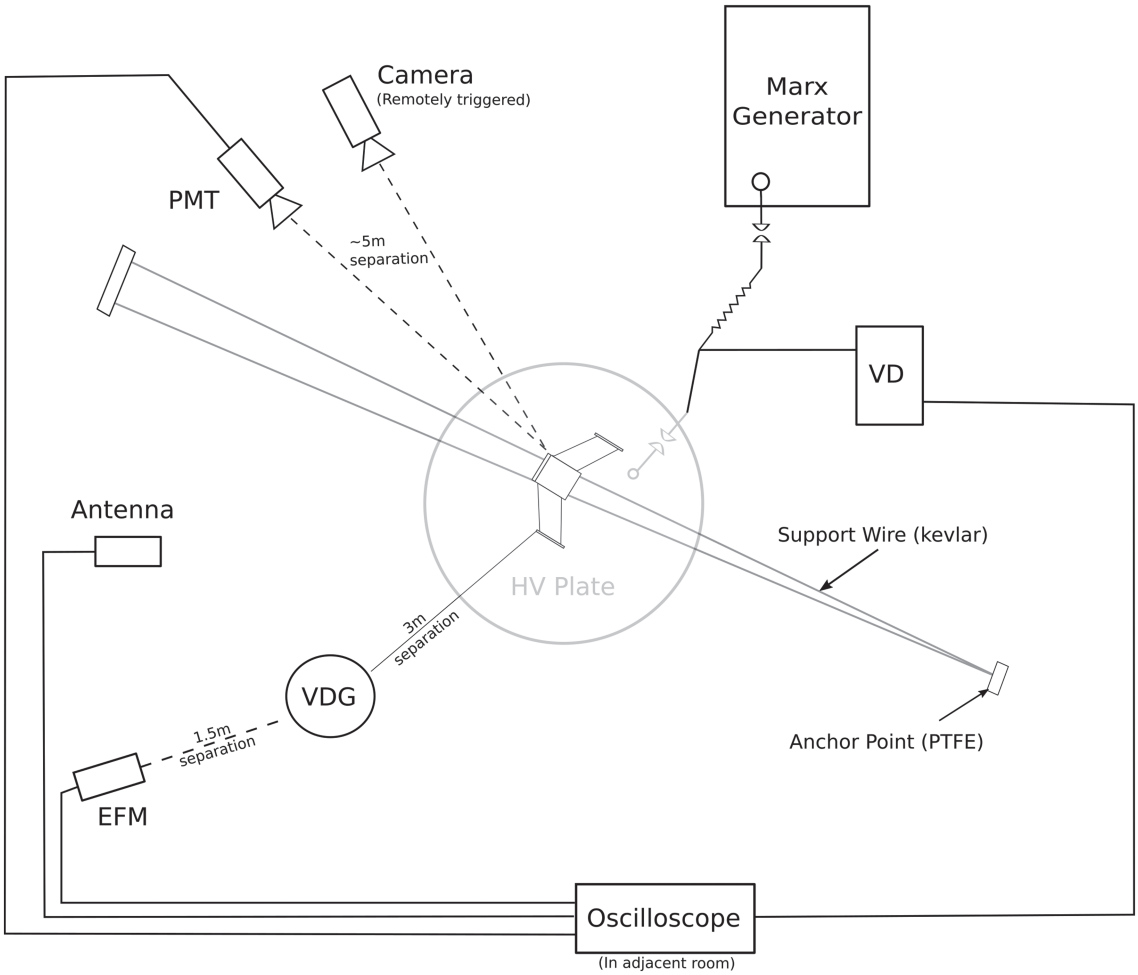

Figure 3. Plan view of experimental setup showing approximate location of sensors relative to aircraft model.

0.3 and 2.7ms. In all cases where a breakdown was observed, it occurred near the waveform peak, and at a time when the spark gap was closed.

Five sensors were used for diagnostics. First, a voltage divider was connected to the high-voltage side of the circuit at the location indicated in Figure 2 in order to measure the applied potential. Second, a camera set to capture long-exposure (3s) images and equipped with a UV lens was pointed at the model. This device was used to visually determine whether any discharge had occurred. To supplement this, a photomultiplier tube (PMT) with a UV band-pass filter was pointed at the location on the model, where the first leader was expected. This measurement was able to time-resolve the discharge, although the very intense luminosity would often saturate the detector after leader connection between the model and the high-voltage electrode. Also used to detect the leader was an antenna, which measured variations in the ambient electric fields caused by leader propagation/current flow. The antenna was a flat plate antenna with gain −60 dB and bandwidth 400 Hz to 500 MHz. The final sensor was an electric field mill (EFM), which was pointed at the Van de Graaff generator and as far as possible from the parallel plate electrodes. The primary purpose of this sensor was to determine the level of charge on the model, as charged by the Van de Graaff generator. The field mill was calibrated by applying a known voltage to the spherical electrode of the Van de Graaff generator using a high-voltage power supply and measuring the output signal. The field mill was calibrated to be accurate for electrode voltages between 0 and −50kV since this was the typical range applied using the Van de Graaff generator.

2.3. Interpretation of the Sensor Data

Each sensor is capable of detecting leader formation on its own and also provides unique information when the output of all sensors is combined. An example of a positive leader trace is shown in Figure 5. The leader

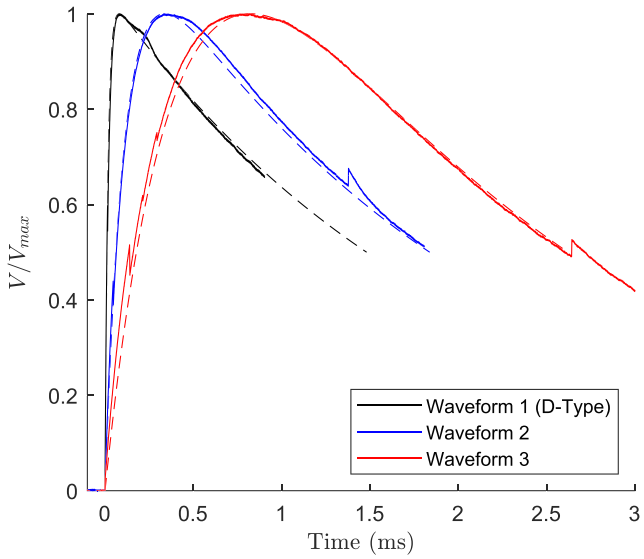

Figure 4. Voltage waveforms used in tests with normalized amplitude. Dashed lines are idealized waveforms; solid lines are measured signals. The rise times, defined as the time to peak, are 90, 330, and 800μs for waveforms 1, 2, and 3, respectively.

is first identified by the PMT and the antenna at point A. The signal is attributed to a leader, and not streamers, due to the high luminosity: Streamers are typically less bright than leaders. Since a voltage change is not measured in the high-voltage plate, this indicates that the leader is originating at the aircraft model. This is consistent with the physics of real aircraft-triggered lightning (Lalande & Delannoy, 2012; Plumer, 2012). After approximately 5μs (point B), the upper plate voltage begins to change. This indicates that the leader has bridged the gap, and that current is flowing from the high-voltage plate to the model. The 5μs transit time across a gap on the order of 25cm gives a leader speed of $5 \cdot 10^4 m/s$. A leader speed on the order of $10^4 m/s$ is consistent with other laboratory measurements (Andreev et al., 2008; Les Renardieres Group,

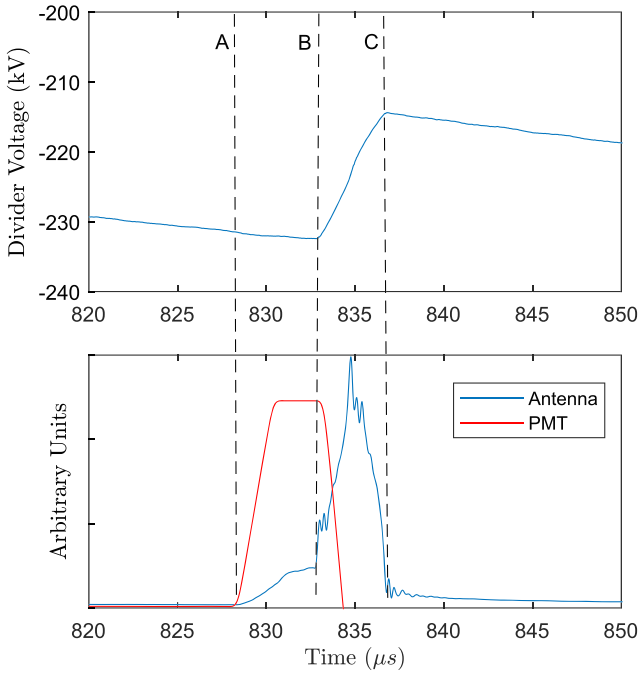

Figure 5. Sensor signals representative of positive leader inception and propagation. (A) Leader initiation point; (B) leader connection to HV plate; (C) spark termination.

Figure 6. Representative photograph of aborted positive leader originating from model (3s camera exposure). The total length of this aborted leader, measured along the leader path and accounting for its tortuosity, is 44cm.

1973; Plumer, 2012) and further evidence that the signal being observed is a positive leader. Note that the sensitive PMT saturates due to the bright leader between points A and B. At point B, when the even brighter spark connects, the PMT starts reading over-range, which is why the signal cuts out. The current flow lasts a few microseconds during which the antenna picks up significant changes in the surrounding electric fields relative to those occurring during leader propagation. After the model and plate have equilibrated, the current flow stops, and the system begins to settle (point C). To visually confirm what type of discharge had occurred (none, aborted leader, or gap-bridging leader), the long exposure UV-sensitive camera was used. This camera was set to 3s exposure and triggered immediately before the high-voltage impulse. An example of an aborted leader is shown in Figure 6, and an example of a gap-bridging leader (spark) is shown in Figure 7.

Note that the positioning of the model within the discharge gap as shown in Figure 7 was selected to hinder the propagation of the second leader. Second leader propagation was undesirable because it would lead to full breakdown in the gap, which would saturate the camera and PMT and make analysis difficult, as well as potentially damage the Van de Graaff generator. In the configuration chosen, the second leader is unlikely to form for two reasons. First, the theoretical model of section 4 shows that, even after connection of the positive leader with the high voltage plate, the negative inception threshold is not reached (see section 4.2). Second, the peak amplitudes delivered by the Marx generator in the tests were below the breakdown value

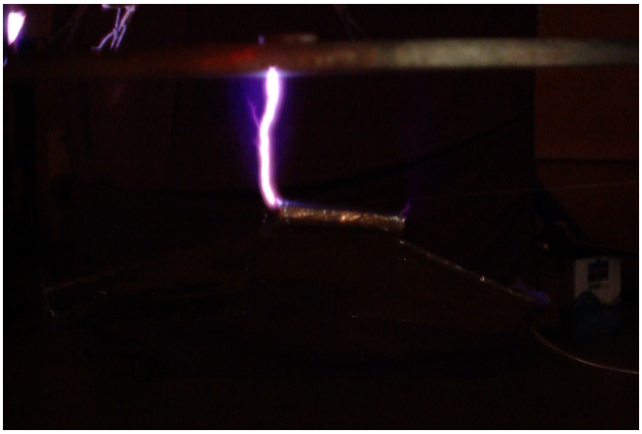

Figure 7. Representative photograph of gap-bridging positive leader originating from model (3s camera exposure). The gap bridged by the leader in this configuration was 26cm.

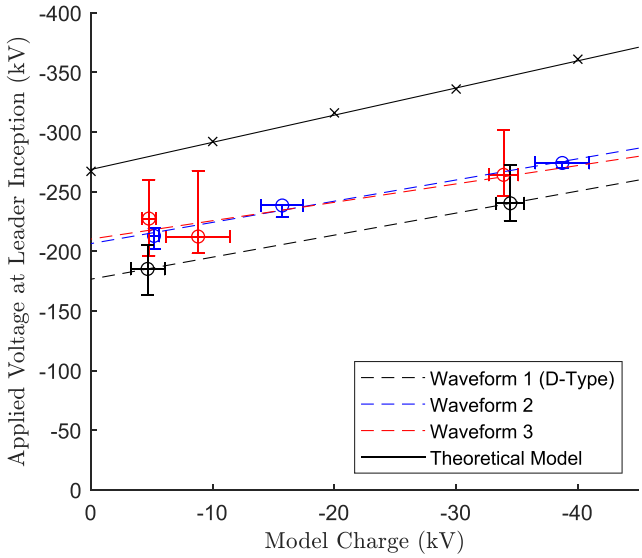

Figure 8. Measured breakdown threshold for 3 voltage waveforms as a function of model voltage. Error bars on charge correspond to the maximum and minimum charge levels observed during the tests. Positive error bars on voltage correspond to the highest peak voltage the gap withstood, and negative error bars correspond to the lowest voltage at the start of a gap bridging leader.

of the insulating post supporting the Van de Graaff high voltage electrode, so breakdown in that gap is also avoided.

2.4. Determination of the Breakdown Threshold

The breakdown threshold can be defined in a few different ways. In testing electrical insulation, typical methods consist of applying a series of voltage shots and using statistical analysis techniques to determine the voltage at which the insulation has a 50% chance of breaking down. Some of these methods are discussed in Kuffel et al. (2000), and this is the method typically used by Labelec, the facility where the experiments were performed. In regards to leader formation, it is possible to identify the precise voltage at which the first leader is incepted using the analysis discussed in section 2.3 and shown in Figure 5. In every case where a leader was observed, the measured voltage of the upper plate electrode at the moment of leader inception, point A in Figure 5, was recorded. The average of these measurements was used as the threshold for leader formation. An up and down method similar to the one described in Kuffel et al. (2000) with at least 10 shots was applied to the Marx generator. This was necessary because the leader initiation voltage depends on the voltage rise rate as will be shown later in this work, so it was important to vary the peak value of the waveform.

3. Experimental Results

3.1. Net Charge Effect on Breakdown Voltage

Tests were performed using each of the waveforms shown in Figure 4, with a minimum of 10 shots per configuration. In the cases where a leader bridged the gap between the model and the plate (Figure 7), the leader inception voltage was determined since these cases correspond to a viable positive leader. The results were averaged across all tests in a given configuration.

The value reported for the model voltage was measured around $100\mu s$ before the Marx generator was triggered, using the field mill pointed at the Van de Graaff generator. The model charge did not vary significantly in the interim between the Marx generator being triggered and the positive leader generation (point A in Figure 5), with absolute differences typically less than 500V. For the example in Figure 5, the difference between the model voltage before the Marx generator is triggered, and that measured at point A is less than 1%.

Figure 8 shows that, as the model acquires more negative charge, the threshold for first (positive) leader formation increases in magnitude. This outcome confirms the influence of vehicle net charge on the likeli-

Table 1
Slope of the Breakdown Versus Model Charge Curve for the Different Waveforms (Rise Times in Parentheses)

Waveform	Slope (kV/kV)
1 (90μs)	1.85
2 (330μs)	1.78
3 (800μs)	1.54
Theoretical model	2.28

hood of lightning strike occurrence, as predicted by Guerra-Garcia et al. (2018). A direct comparison with the theoretical model is discussed in section 4.2.

A linear fit to the data is shown, and the slopes are recorded in Table 1. The fit has a positive slope greater than unity for all three waveforms tested. In all cases, the slope of the curves shows reasonable agreement with the theoretical breakdown curve, with the discrepancy in slope and breakdown voltage attributable to different model geometry and other uncertainties in the model discussed in the original paper (Guerra-Garcia et al., 2018).

It is interesting to note that in those tests with a model aircraft that had been grounded, a potential of approximately −5kV developed on the model during the time between grounding and the start of the voltage pulse. For safety reasons, the grounding (which was done manually) had to be performed well in advance of the high-voltage shot. One possible explanation for this baseline charge is charge conduction by the insulating support cables, which were found to have nonzero conductance when high voltage was applied across them. Charge could accumulate in these cables during the last voltage shot and be conducted to the model. Residual space charge from the previous voltage shot could also be a factor in creating the baseline charge. It is of interest to note that, as far as the authors know, the standard recommended practices do not discuss the need of grounding the model in between tests and the present results show the criticality of this good practice.

When extrapolating the test results to the airborne scenario, some discrepancies may exist related to the effect of negative coronae that will be developing on the negatively charged model prior to the high-voltage impulse, due to the model's high voltage relative to the surroundings. An estimate of the onset voltage of these coronae is discussed later (section 3.3). In the tests, the presence of these negative ions in the vicinity of the model could be modifying the conditions for leader initiation in a way not entirely consistent with the airborne situation. Note that this ion cloud is not expected to interfere with the EFM measurement, since the measurement is taken about 3m away from the model (see Figure 3). Another difference between the lab and airborne situations is the effect of nearby grounded objects causing the experimental setup to deviate from the idealized situation wherein the aircraft is exposed to a uniform applied field and is far away from other objects.

3.2. Effect of Voltage Rise Rate

In reality, aircraft-triggered lightning will occur both for aircraft exposed to a rapid rise in the ambient field (e.g., due to nearby lightning, Saba et al., 2016) and for aircraft flying into sufficiently high ambient fields (in-flight experiments report ambient fields about 50 kV/m at the moment of triggered-lightning, Rakov & Uman, 2003). Considering that a typical airliner flies about 250 m in 1 s, and this may be of the order of the motion required to enter the area of influence of a cloud charge center, the conditions might be *slow* in the second scenario compared to the waveforms tested. However, fast waveforms need to be used in laboratory tests to compensate for static electrodes and simulate to some extent that a fast-moving aircraft can escape regions of space charge, created by local corona phenomena, modifying the conditions for leader formation. E.g., it has been observed that initiation of upward leaders from rotating blades of windmills occurs more readily than from static towers due to the redistribution of the ion charge cloud that locally shields the electric fields in static towers (Montanya et al., 2014).

When comparing the three waveforms tested, with rise times ranging between 90 and 800μs, the threshold for leader formation is reduced when the rate of voltage rise is increased. This effect is most noticeable when comparing waveform 1 (90μs, D-type) to waveforms 2 (330μs) and 3 (800μs) and is seen for all charging levels. The breakdown threshold, at comparable charging levels, for waveform 3 was about 30 kV in magnitude less than for the faster waveforms. As discussed in section 2.1, it is known (Les Renardieres Group, 1973)

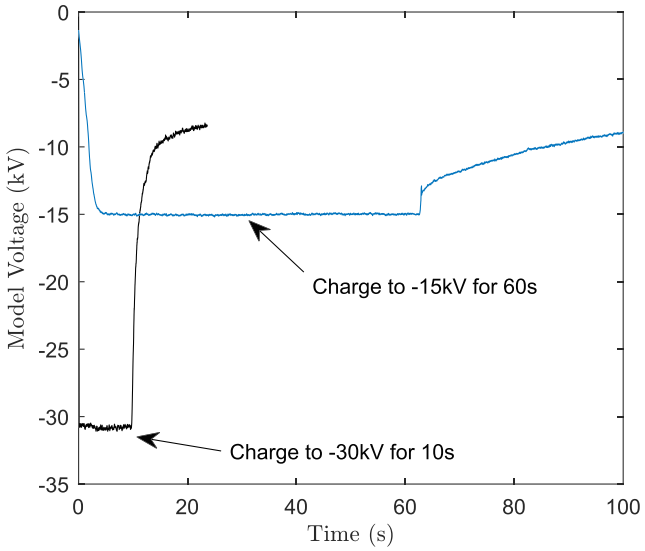

Figure 9. Model discharging curves for model charged to –30 and –15kV.

that the rate of field rise has an impact on breakdown characteristics, and it appears that extending the rise time beyond that of the standard D-type waveform increases the breakdown threshold.

The data for waveform 3 show some unexpected results, notably the large error bars and inconsistent trend at low voltages. Part of the issue here is the slow ramp in waveform 3, which was difficult to achieve experimentally. These tests yielded a signal that indicated that the spark gap between the Marx generator and the high-voltage plate electrode would turn on and off during the voltage ramp, while in the other tests performed the circuit to the plate remained closed after the initial connection was made. One instance of this spark gap switching can be seen in the rise portion of waveform 3 when compared to the idealized waveform in Figure 4. The result was a voltage application to the plate electrode that occurred in steps, rather than a smooth ramp, obstructing the interpretation of the results.

More interestingly for the range of rise times tested, it is shown in Figure 8 and Table 1 that the variation of the breakdown potential with model charge (the slope of the line) is only weakly related to the rate of rise of the input voltage, and the weak dependence observed is within the margin of error of the experimental data. This means that a negatively charged model hinders positive leader inception by about the same amount regardless of the rate of rise of the external field.

3.3. Model Aircraft Discharging

For the chosen aircraft model, it was difficult to maintain a voltage on the model beyond a few tens of kilovolts, without a continuous current supply. At voltages on the order of –10 to –15kV, the sharp corners on the model (or possibly wrinkles in the aluminum foil) would begin to corona emit, dissipating the charge. This effect was observed visually through long-exposure photographs taken with a UV-sensitive lens, as well as through a noncontact measurement of the model voltage, once the charging source was disconnected. An example of this measurement is shown for two tests in Figure 9. In both cases, immediately after the charging source was disconnected, the model aircraft began to rapidly discharge. The slope of this discharging curve became less steep when the model had dropped to around –10 or –12kV depending on the test. This is interpreted as a termination of the corona emission mechanism from the aircraft extremities and the dominant discharge mechanism switching to conduction through the support cables. The time constants corresponding to the fast and slow discharging mechanisms, τ_{fast} and τ_{slow}, can be estimated by fitting the data in Figure 9 by a double exponential decay:

$$V = V_{\text{fast}} \exp(-t/\tau_{\text{fast}}) + V_{\text{slow}} \exp(-t/\tau_{\text{slow}}).$$

An estimate of these time constants is given in Table 2. There are two important conclusions to be drawn from this figure. First, to maintain a model voltage beyond –10kV requires an *active* charging strategy that

Table 2
Time Constants for Model Discharging

Initial charge (kV)	$\tau_{fast}(s)$	$\tau_{slow}(s)$
−30	0.92	31
−15	0.29	74

remains connected at the moment of the high-voltage impulse. Second, while conduction through the insulating support cables is significantly less rapid than the corona discharge mechanism, it is nonzero during high-voltage testing.

4. Discussion Guided by Comparison to Electrostatic Model

4.1. Computational Model Description

A physics-based numerical model is used to explain the experimental observations. The model is described in detail in (Guerra-Garcia et al., 2017, 2018) and is based on the numerical zoning methods developed by Lalande et al. (1999a) that combine an electrostatic simulation of the aircraft to semiempirical criteria for leader inception. The semiempirical leader inception criteria used are based on the critical charge concept of Gallimberti (1979): A leader is incepted if the charge accumulated within the impulse corona that precedes the leader exceeds a certain threshold (q_{cr}). The corona charge is estimated from the electrostatic model through a volumetric integral (Arevalo et al., 2012) assuming that the electric field within the corona is constant and equal to the stability field value, E_{cr} (Gallimberti, 1979). The main difference between this model and those previously reported in the literature is that it makes no assumption on the polarity of the first leader to be incepted and uses different thresholds for the positive and negative polarity. The thresholds used for the positive leader inception are $q_{cr}^{+} = 1\mu C, E_{cr}^{+} = 450kV/m$; and for the negative leader: $q_{cr}^{-} = -4\mu C$, $E_{cr}^{-} = 750kV/m$ (consistent with laboratory measurements by Castellani et al. (1998) and Niemeyer (1991) and theoretical work by Gallimberti et al. (2002), among others). For self-consistency, the model is briefly described in what follows.

4.1.1. Determination of Breakdown Voltage and First Attachment Point

The prestrike electrostatics of the model aircraft at a pitch angle of 50 degrees placed between two large parallel plates at a distance of 145cm, as pictured in Figure 2, is solved by solving Laplace's equation. The bottom plate is grounded, and a negative high-voltage potential is applied to the upper plate. The geometry of the model used is that in Guerra-Garcia et al. (2018), scaled to have the same wingspan as in the experiment in order to have a comparable electrical capacitance of value $C = 41$pF in the numerical model.

The prestrike electrostatics are solved for a given net charge of the vehicle (in the computational model, the net charge and voltage are related through the capacitance), and the voltage of the upper plate is gradually increased in amplitude. At each upper-plate voltage level, the criteria for both positive and negative leader inception are tested on all possible attachment points (namely nose, wing tips, and rear end). Once the criterion for leader inception has been reached at any given point, the first attachment point and the applied voltage for leader inception has been obtained.

4.1.2. Propagation of First Leader and Second Attachment Point

Once the first leader is incepted, it propagates along the local electric field line with a constant charge per unit length, $\lambda^{+} = 65\mu C/m$ for the positive leader and $\lambda^{-} = 108\mu C/m$ for the negative leader, as measured by Les Renardieres Group (1973). As the leader propagates, the net charge of the model, Q, is biased in the opposite polarity:

$$Q(t) = Q(0) \mp \lambda l(t),$$

where the minus sign corresponds to the case of a positive leader preceding, time zero corresponds to first leader inception, and $l(t)$ is the length of the leader at each moment. At each time step, the criterion for the opposite polarity leader inception is tested on all possible attachment points. As the model is biased in the direction that favors the opposite polarity leader, the first leader is propagated in time until the second leader is triggered.

4.2. Computational Model Results and Comparison to Experimental Data

The computational model is used to explain the experimentally measured influence of model net charge on self-triggered lightning (section 3.1).

Table 3
Breakdown Conditions as a Function of the Aircraft Model's Electrostatic Potential (or Equivalently, Its Net Charge), Results of Electrostatic Simulation

ϕ_M [kV]	Q [μC]	First Leader	Second Leader	V_{app} [kV]	l_1^{crit} [cm]
0	0	(+) Nose	(–) Nose	–267	21.9
–10	–0.4	(+) Nose	(–) Wing tip	–292	21.2
–20	–0.8	(+) Nose	(–) Rear end	–316	20
–30	–1.2	(+) Nose	(–) Rear end	–336	18.8
–40	–1.6	(+) Nose	(–) Rear end	–361	17.5
–50	–2.1	(+) Nose	(–) Rear end	–381	16.3
–60	–2.5	(+) Nose	(–) Rear end	–402	15.1
–70	–2.9	(+) Nose	(–) Rear end	–420	14
–80	–3.3	(+) Nose	(–) Rear end	–445	12.6
–120	–4.9	(+) Nose	(–) Rear end	–526	7.5
–150	–6.2	(+) Nose	(–) Rear end	–583	3.8
–170	**–7.0**	(+) Nose	(–) Rear end	**–624**	**1.2**
–190	–7.8	(–) Rear end	(+) Nose	–616	0.9
–200	–8.2	(–) Rear end	(+) Nose	–599	1.7
–225	–9.2	(–) Rear end	(+) Nose	–551	3.5

Table 3 shows the influence of model potential ϕ_M (note that it relates to the net charge Q through the self-capacitance) on the voltage applied to the upper plate, V_{app}, to trigger a bidirectional leader. The first leader and its polarity, as well as the second leader and the length of the first leader at second leader inception (l_1^{crit}) are also reported. The first five rows correspond to the range experimentally tested.

For an uncharged model, $\phi_M = 0$, the first leader to be incepted is the positive one, since the threshold values in the positive polarity are lower than in the negative polarity. The experimentally measured voltage for positive leader inception is approximately 30–35% lower than the model predicts. The first attachment point predicted by the model, as in the experiment, is at the nose of the vehicle. As the positive leader propagates, it biases the vehicle to negative values facilitating the inception of the negative leader. The model predicts the initiation of the negative leader occurs when the first leader is $l_1^{crit} \approx 22$ cm long. This translates to the model being biased to $\phi_M(l_1^{crit}) = C^{-1}Q(l_1^{crit}) = -347$kV. The implications for the experiment are that, since this magnitude is higher than the peak amplitudes delivered by the Marx generator in the tests and the gap between vehicle and upper plate is comparable to the critical distance, the second leader will not be triggered from the model, even after the first leader connects to the upper plate.

As the model aircraft charge, Q, and potential, ϕ_M, are made more negative, the conditions for the positive leader inception are made more difficult, and those for negative leader inception are favored. This results in an increase in the applied voltage to trigger the first leader, and a reduced first leader propagation length to bias the aircraft to the level required for second leader inception. Despite the offset in breakdown threshold in the uncharged case between the experiment and model (Figure 8), the slope of the breakdown voltage to charging level curve is in reasonable agreement, see Table 1. Note that, aside from the simplifications of the model, the geometries of the vehicles and experimental setup are not identical, and the empirical parameters are only roughly known.

Table 3 is extended to determine the net vehicle charge that makes leader inception hardest: This is the optimum condition in terms of lightning avoidance, and it is marked in bold font. Beyond this level, at $\phi_M = -170kV$, the conditions are such that the positive leader is suppressed, and the negative leader becomes more likely; the applied voltage required to trigger it can again be reduced. For net charge levels above this value, the positive leader precedes; for lower net charge levels, the negative leader is incepted first. Therefore, the optimum corresponds to the case when both leaders are simultaneously incepted.

Note that in the experimental setup it was not possible to reach such high vehicle net charge levels since the charging strategy needs to compensate for any natural coronae formed at the extremities of the vehicle (see

section 3.3). In the experimental scenario, this charging speed was limited by the velocity of the charging belt of the Van de Graaff generator.

5. Lightning Detection, Prediction, and Risk Reduction

The experiments reported in this paper have shown that aircraft net charge has a strong influence on lightning inception. In addition, electrostatic signals and models could be used for *lightning detection and prediction* and ultimately, a charge control system could be implemented to minimize the risk of a strike (Martinez-Sanchez et al., 2019).

One key element to the successful implementation of such a charge control strategy is the ability to charge the aircraft during flight to the desired levels. Lalande et al. (1999b) indicates that charges on the order of a millicoulomb can naturally develop on aircraft flying in an environment conducive to lightning strikes. The capacitance of the aircraft in question was on the order of a nanofarad, which implies a voltage on the order of a megavolt (typically negative relative to the surroundings). More interestingly, artificial charging of a B-17 research aircraft was demonstrated by Stimmel et al. (1946) and Waddel et al. (1946) using emission of positively charged droplets from the aircraft surface to a potential of about –0.5MV, which corresponds to a net charge of –0.4mC. Other experiments using smaller aircraft and ion emission have demonstrated artificial charging to 20–40 μ C levels (negative) (Jones, 1990). Note that the charging levels that led to a measurable impact on the breakdown conditions for the 1m wingspan model vehicle in the laboratory setup were of the order of 1μC (negative) or –30kV. The modeling work in section 4 suggests a scaling of this charge quadratic with size or equivalently a linear scaling of the potential with size: E.g., a ~30m wingspan aircraft would require charging levels of the order of 1mC or ~1MV (Guerra-Garcia et al., 2018).

Another necessary element of this strategy is the ability to have a reasonable prediction of leader inception before it occurs. Currently, aircraft operations in lightning conditions are informed by the onboard weather radar, communications between pilots, and contact with Air Traffic Control (ATC). Moreover, flight operations manuals rarely mention lightning but rather thunderstorms alone.

Aircraft weather radar typically displays storm cell information although modern, proprietary, technologies integrate distinct "lightning icons." These technologies are designed to detect electrical discharge activity that the radar cannot see and map the lightning activity onto the weather radar display of the pilot (Honeywell, 2016).

Contact with ATC provides additional weather data (mainly related to thunderstorm development) but may also include direct lightning observations by Lightning Detection Networks (LDNs). For example, the National LDN detects cloud-to-ground flashes with an efficiency of 90–95%. Information of lightning detectors based on RF emissions are often included in METAR (MEteorological Terminal Aviation Routine) weather reports as an indicator of the nearby presence of a thunderstorm (Transportation Research Board and National Academies of Sciences, Engineering, and Medicine, 2008). Note that the information based on weather reports and LDN summarize the current or recent scenario, rather than what comes ahead. *Prediction* technologies include monitoring the growth and motion of convective systems that can develop into thunderstorms using *nowcasting* techniques by measuring, using radar and satellites, storm properties (Mäkelä et al., 2013). These are used by the FAA for both en route and terminal air traffic management.

Note that around 40% of lightning strikes reported by airline pilots are experienced with no thunderstorms in the immediate area (Sweers et al., 2012), which suggests that the presence of thunderstorms alone is not a good indicator of the incidence of aircraft-triggered lightning.

Other existing technologies, not currently used to predict lightning to aircraft, include Total Lightning Systems that are able to detect both cloud-to-ground (CG) lightning and intra-cloud (IC) lightning. Optical detectors onboard geostationary meteorological satellites (e.g., the Geostationary Lightning Mapper onboard the Geostationary weather satellites GEOS-16 and the Meteosat Third Generation Lightning Imager MTG-LI) are able to provide this information. In addition, electric field mills can be used to alert of a possible threat (*predicting* rather than *detecting* a strike after it occurs). For that reason, electric field mills are a key component of the launch evaluation systems employed at NASA's Kennedy Space Flight Center. Only research aircraft have carried electric field mills onboard, and these sensors are not routinarily used in aviation (Fisher & Plumer, 1984).

6. Conclusions

This paper presented an experimental study of the effect of aircraft net charge on its susceptibility of being struck by lightning. The threshold background electric field for leader initiation was shown to increase (in magnitude) as the aircraft accumulated a greater amount of negative electric charge. Note that the trend applies to the specific orientation of the electric field tested (vertical field, vehicle pitched at 50°). This effect was observed for different rates of rise of the ambient electric field (from 90 to 800μs), including one that is consistent with standard lightning leader attachment tests. Use of slower waveforms, e.g., representative of an aircraft entering an area of influence of a cloud charge center, was hindered by experimental constraints. For the waveforms tested, the breakdown threshold increased approximately linearly with the amount of charge applied to the aircraft model and showed reasonable agreement with simulations. These results verify both the validity of the methods employed in those simulations and the potential of using charge control as a means of reducing the risk of aircraft-triggered lightning. When implemented as part of a larger system of lightning detection and prediction, active charge control of aircraft is a promising strategy to help prevent costly strikes from occurring.

Acknowledgments
This collaboration was supported by the MIT-Spain La Caixa Foundation Seed Fund (MISTI Global Seed Funds grant program). The experiments were performed at Labelec Lightning Labs, Terrassa (Barcelona), Spain, and the authors would like to thank G. Tobella for his contributions to the experimental campaign. The MIT team acknowledges partial support from The Boeing Company through the Strategic Universities for Boeing Research and Technology Program. This work was also supported in part by research grants from the Spanish Ministry of Economy and the European Regional Development Fund (FEDER): ESP2015-69909-C5-5-R and ESP2017-86263-C4-2-R, also by ENE2017-91636-EXP. The authors would like to thank P. Kochkin (University of Bergen) for contributions to the preliminary experiments and O. van der Velde (U. Politècnica de Catalunya) for his help with the photography of the discharges. The data presented in this paper can be found in DSpace@MIT, in the "Data Related to Publications" collection (https://dspace.mit.edu/handle/1721.1/122360).

References

Andreev, A. G., Bazelyan, E. M., Bulatov, M. U., Kuzhekin, I. P., Makalsky, L. M., Sukharevskij, D. I., & Syssoev, V. S. (2008). Experimental study of the positive leader velocity as a function of the current in the initial and final-jump phases of a spark discharge. *Plasma Physics Reports*, *34*(7), 609–615.

Arevalo, L., Cooray, V., Wu, D., & Jacobson, B. (2012). A new static calculation of the streamer region for long spark gaps. *Journal of Electrostatics*, *70*, 15–19.

Bixler, J., & Sponholz, D. (2016). FT Spear Plans. https://store.flitetest.com/flite-test-spear-electric-airplane-kit-1041mm-flt-1043/p673707

Castellani, A., Bondiou-Clergerie, A., Lalande, P., Bonamy, A., & Gallimberti, I. (1998). Laboratory study of the bi-leader process from an electrically floating conductor. Part 2: bi-leader properties. *IEE Proceedings - Science, Measurement and Technology*, *145*(5), 193–199.

EUROCAE (2005). ED-105 Aircraft Lightning test Methods. EUROCAE.

Fisher, F. A., & Plumer, J. A. (1977). Lightning protection of aircraft. NASA Reference Publication 1008, https://ntrs.nasa.gov/archive/nasa/casi.ntrs.nasa.gov/19780003081.pdf

Fisher, B. D., & Plumer, J. A. (1984). Lightning attachment patterns and flight conditions experienced by the NASA F-106B airplane from 1980 to 1983. AIAA 22nd Aerospace Sciences Meeting (Reno, Nevada, Jan. 9-12) No. AIAA 84–0466.

Gallimberti, I. (1979). The mechanism of the long spark formation. *Journal de Physique Colloques*, *40*(C7), 193–250.

Gallimberti, I., Bacchiega, G., Bondiou-Clergerie, A., & Lalande, P. (2002). Fundamental processes in long air gap discharges. *C. R. Physique*, *3*, 1335–1359.

Guerra-Garcia, C., Nguyen, N. C., Peraire, J., & Martinez-Sanchez, M. (2017). Influence of net charge on the probability of lightning initiation from aircraft. In *Proceedings of the 2017 International Conference on Lightning and Static Electricity (ICOLSE)*, Nagoya, Japan.

Guerra-Garcia, C., Nguyen, N. C., Peraire, J., & Martinez-Sanchez, M. (2018). Charge control strategy for aircraft-triggered lightning strike risk reduction. *AIAA Journal*, *56*(5), 1988–2002.

Honeywell (2016). Technical white paper IntuVue(R) RDR-4000 3D Weather Radar Systems. https://aerospace.honeywell.com

Jones, J. J. (1990). Electric charge acquired by airplanes penetrating thunderstorms. *JGR. Journal of Geophysical Research. Part D, Atmospheres*, *95*(10), 16.589–16.600.

Kasemir, H. W. (1950). Qualitative Uebersicht ueber Potential-Feldund Ladungsverhaltnisse bei einer Blitzentladung in der Gewitterwolke. In Das Gewitter, ed. Hans Israel, Akad. Verlags. Ges. Geest and Portig K.-G, Leipsig, Germany.

Kuffel, E., Zaengl, W. S., & Kuffel, J. (2000). 8.4.7 laboratory test procedures. https://app.knovel.com/hotlink/khtml/id:kt00BJPES8/high-voltage-engineering/laboratory-test-procedures

Lalande, P., Bondiou-Clergerie, A., & Laroche, P. (1999a). Computations of the initial discharge initiation zones on aircraft or helicopter. In *Proceedings of the 1999 International Conference on Lightning and Static Electricity (ICOLSE), Toulouse, France*.

Lalande, P., Bondiou-Clergerie, A., & Laroche, P. (1999b). Analysis of available in-flight measurements of lightning strikes to aircraft. In *Proceedings of the 1999 international conference on lightning and static electricity (icolse), toulouse, france*.

Lalande, P., & Delannoy, A. (2012). Numerical methods for zoning computation. Journal Aerospace Lab Issue 5, AL05–08.

Les Renardieres Group (1973). Research on long gap discharges at Les Renardieres. Electra 35.

Mäkelä, A., Saltikoff, E., Julkunen, J., Juga, I., Gregow, E., & Niemelä, S. (2013). Cold-season thunderstorms in Finland and their effect on aviation safety. *Bulletin of the American Meteorological Society*, *94*(6), 847–858.

Martinez-Sanchez, M., Guerra-Garcia, C., Nguyen, N. C., Peraire, J., & Mouratidis, T. (2019). Charge control system to reduce risk of an aircraft-initiated lightning strike. Massachusetts Institute of Technology, Cambridge, MA, U. S. Patent No. 10450086, issued Oct. 22, 2019.

Mazur, V. (1988). Lightning initiation on aircraft in thunderstorms. AIAA 26th Aerospace Sciences Meeting (Reno, Nevada, Jan. 11-14), No. AIAA 88-0391.

Mazur, V. (1989). A physical model of lightning initiation on aircraft in thunderstorms. *Journal of Geophysical Research*, *94*(D3), 3326–3340.

Montanya, J., van der Velde, O., & Williams, E. R. (2014). Lightning discharges produced by wind turbines. *Journal of Geophysical Research: Atmospheres*, *119*, 1455–1462. https://doi.org/10.1002/2013JD020225

Moreau, J. P., Alliot, J. C., & Mazur, V. (1992). Aircraft lightning initiation and interception from in situ electric measurements and fast video observations. *Journal of Geophysical Research*, *95*(15), 903–12.

Niemeyer, L. (1991). *Gaseous dielectrics IV. Section on Leader breakdown in compressed SF_6: recent concepts and understanding*, pp. 49–60. New York: Plenum Press.

Plumer, J. A. (2012). Laboratory test results and natural lightning strike effects: How well do they compare. In *International conference on lightning protection*. Vienna, Austria.

Plumer, J. A. (2017). Lightning and aircraft: an incomplete history of research and standardization. In *Proceedings of the 2017 International Conference on Lightning and Static Electricity (ICOLSE)*. Nagoya, Japan.

Rakov, V. A., & Uman, M. A. (2003). *Lightning Physics and Effects*. Cambridge: Cambridge University Press.

Reazer, J. S., Serrano, A. V., Walko, L. C., & Burket, H. D. (1987). Analysis of correlated electromagnetic fields and current pulses during airborne lightning attachments. *Electromagnetics*, *7*, 509–39.

SAE Aerospace (2005). SAE ARP5416. SAE International.

SAE Aerospace (2012). SAE ARP5414A. SAE International.

SAE Aerospace (2013). SAE ARP5412B. SAE International.

Saba, M., Schumann, C., Warner, T. A., Ferro, M. A. S., Paiva, A. R., Heldson Jr, J., & Orville, R. E. (2016). Upward lightning flashes characteristics from high-speed videos. *Journal of Geophysical Research: Atmospheres*, *121*, 849–8505. https://doi.org/10.1002/2016JD025137

Stimmel, R. G., Rogers, E. H., Waterfall, F. E., & Gunn, Ross (1946). Army-navy precipitation-static project: Part III-electrification of aircraft flying in precipitation areas. *Proceedings of the IRE*, *34*(4), 167–177.

Sweers, G., Birch, B., & Gokcen, J. (2012). Lightning strikes: Protection, inspection, and repair. *AERO Magazine*, *QTR 4*, 19–28.

Transportation Research Board and National Academies of Sciences, Engineering, and Medicine (2008). *Lightning-warning systems for use by airports*. Washington, DC: The National Academies Press.

Uman, M. A. (2008). *The art and science of lightning protection*. Cambridge: Cambridge University Press.

Vonnegut, B., & Little, A. D. (1965). Electrical behavior of an airplane in a thunderstorm. Technical Report for Federal Aviation Agency, FAA-ADS-36.

Waddel, R. C., Drutowski, R. C., & Blatt, W. N. (1946). Army-navy precipitation-static project: Part II-aircraft instrumentation for precipitation-static research. *Proceedings of the IRE*, *34*(4), 161–166.